Carbon Source Starvation of a Sulfate-Reducing Bacterium–Elevated MIC Deterioration of Tensile Strength and Strain of X80 Pipeline Steel

Zhong Li[1], Jike Yang[1,2], Huihua Guo[2], Sith Kumseranee[3], Suchada Punpruk[3], Magdy E. Mohamed[4], Mazen A. Saleh[4] and Tingyue Gu[1]*

[1]Department of Chemical and Biomolecular Engineering, Institute for Corrosion and Multiphase Technology, Ohio University, Athens, OH, United States, [2]Corrosion and Protection Center, University of Science and Technology Beijing, Beijing, China, [3]PTT Exploration and Production, Bangkok, Thailand, [4]Research and Development Center, Saudi Arabian Oil Company, Dhahran, Saudi Arabia

It is known that starved sulfate-reducing bacterial biofilms corrode carbon steel more aggressively because they use electrons from elemental iron oxidation as an alternative source of energy. This work used carbon source starvation to vary MIC (microbiologically influenced corrosion) severity for studying subsequent MIC impacts on the degradation of X80 carbon steel mechanical properties. X80 square coupons and dogbone coupons were immersed in ATCC 1249 culture medium (200 ml in 450-ml anaerobic bottles) inoculated with *Desulfovibrio vulgaris* for 3-day pre-growth and then for an additional 14 days in fresh media with adjusted carbon source levels for starvation testing. After the starvation test, the sessile cell counts (cells/cm^2) on the dogbone coupons in the bottles with carbon source levels of 0, 10, 50, and 100% (vs that in the full-strength medium) were 8.1×10^6, 3.2×10^7, 8.3×10^7, and 1.3×10^8, respectively. The pit depths from the X80 dogbone coupons were 1.9 μm (0%), 4.9 μm (10%), 9.1 μm (50%), and 6.4 μm (100%). The corresponding weight losses (mg/cm^2) from the square coupons were 1.9 (0%), 3.3 (10%), 4.4 (50%), and 3.7 (100%). The 50% carbon source level had the combination of carbon starvation without suffering too much sessile cell loss. Thus, both its pit depth and weight loss were the highest. The electrochemical tests corroborated the pit depth and weight loss trends. The tensile tests of the dogbone coupons after the starvation incubation indicated that sulfate-reducing bacteria (SRB) made X80 more brittle and weaker. Compared with the fresh (no-SRB-exposure) X80 dogbone coupon's ultimate tensile strain of 13.6% and ultimate tensile stress of 860 MPa, the 50% carbon source level led to the lowest ultimate tensile strain of 10.3% (24% loss when compared with the fresh dogbone) and ultimate tensile stress of 672 MPa (22% loss). The 100% carbon source level had a smaller loss in ultimate tensile strain than the 50% carbon source level, followed by 10% and then 0%. Moreover, the 100% carbon source level had a smaller loss in ultimate tensile strength than the 50%, followed by 10% and 0% in a tie. This outcome shows that even in the 17-day short-term test, significant degradation of the mechanical properties occurred and more severe MIC pitting caused more severe degradation.

Keywords: X80 steel, microbiologically influenced corrosion, mechanical property, sulfate-reducing bacteria, tensile test, starvation, biofilm

INTRODUCTION

Sulfate-reducing bacteria (SRB) are the most ubiquitous microorganisms in anaerobic environments, and they are the most important microbes in MIC (microbiologically influenced corrosion) in the oil and gas systems which are mostly anaerobic and often involve seawater containing sulfate (Little and Lee, 2007; Sheng et al., 2007; Xu et al., 2016; Jia et al., 2017; Jogdeo et al., 2017). SRB MIC can induce mechanical degradations of metallic materials (Abedi et al., 2007; AlAbbas et al., 2013; Al-Nabulsi et al., 2015; Wu et al., 2015). A failure of a X52 pipeline in the northern part of Iran was reported in 2004 due to SRB causing deterioration of the mechanical properties of the pipeline steel (Abedi et al., 2007). The deterioration of the mechanical properties is usually exhibited as losses of tensile stress and strain (Służalec, 1992).

The SRB are anaerobic bacteria that use sulfate as the terminal electron acceptor in their respiration (Dannenberg et al., 1992; Heidelberg et al., 2004; Lv and Du, 2018). When lactate is used as the organic carbon source, the following oxidation reaction occurs in the cytoplasm of the SRB under enzyme catalysis (Xu and Gu, 2011; Xu and Gu, 2014; Xu et al., 2016; Li et al., 2018; Dou et al., 2019; Gu et al., 2019):

TABLE 1 | Elemental composition of X80 steel (mass %).

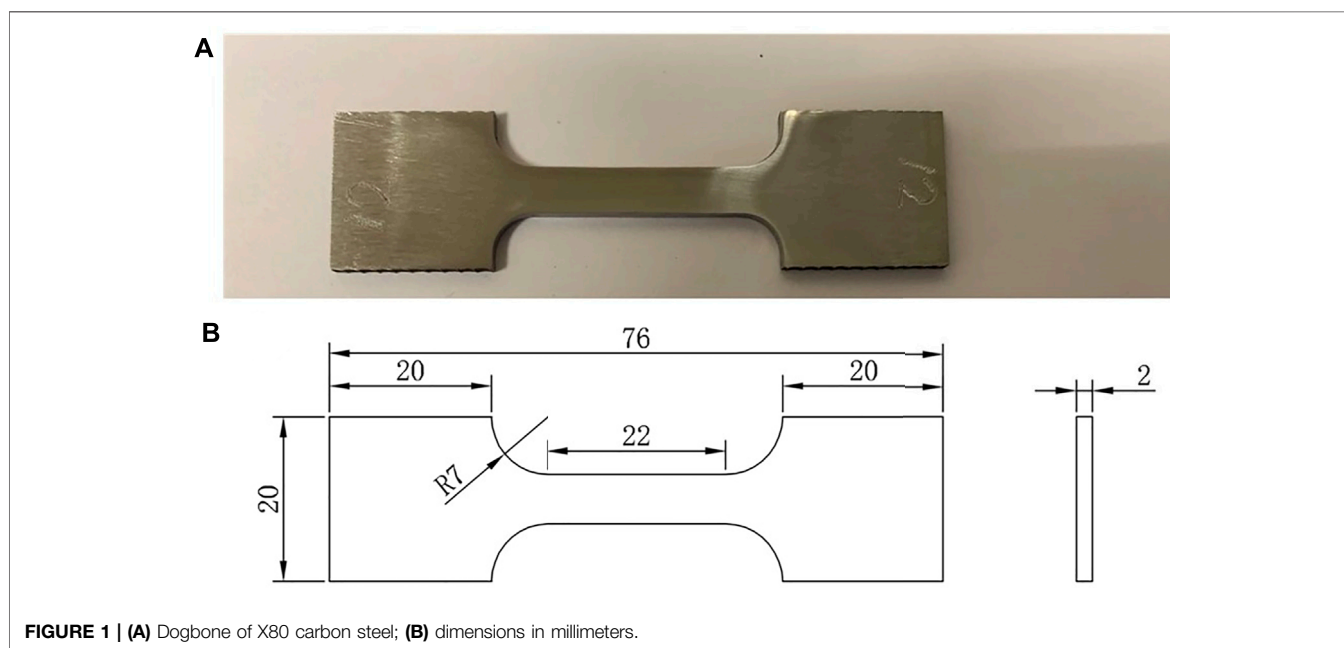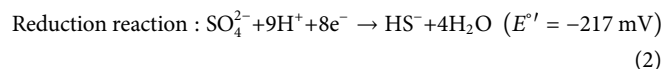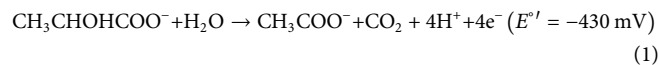| C	Mn	Ni	Cu	Si	Mo	Cr	Nb	Ti	Fe
0.050	1.850	0.285	0.246	0.228	0.307	0.016	0.065	0.013	Balance

**FIGURE 1** | (A) Dogbone of X80 carbon steel; (B) dimensions in millimeters.

TABLE 2 | Chemical composition of ATCC 1249 medium.

Component	Chemical	Amount
Component I	MgSO4·7H$_2$O	4.1 g
	Sodium citrate	5.0 g
	CaSO$_4$	1.0 g
Component II	NH$_4$Cl	1.0 g
	Distilled water	400 ml
	K$_2$HPO$_4$	0.5 g
	Sodium lactate	4.5 ml
	Yeast extract	1.0 g
Component III	Distilled water	400 ml
Component IV	Fe(NH$_4$)$_2$(SO$_4$)$_2$	1.0 g

$$CH_3CHOHCOO^- + H_2O \rightarrow CH_3COO^- + CO_2 + 4H^+ + 4e^- \ (E^{\circ\prime} = -430 \, \text{mV}) \quad (1)$$

$$\text{Reduction reaction}: SO_4^{2-} + 9H^+ + 8e^- \rightarrow HS^- + 4H_2O \ (E^{\circ\prime} = -217 \, \text{mV}) \quad (2)$$

where the apostrophe in the reduction potential E° of the two reactions indicates a pH of 7.0. When there is a lack of carbon source in the local environment such as at the bottom of the sulfate-reducing bacterial biofilm, elemental iron can provide the electrons for the SRB survival through extracellular Fe oxidation, as shown in **Eq. 2**. Fe like lactate can provide

energy according to the reduction potential values listed in **Eqs 1**, **3**. Like lactate, Fe oxidation can be coupled with sulfate reduction to provide energy for SRB (Biswas and Bose, 2005; Li et al., 2018). This means that carbon source starvation of a pre-existing sulfate-reducing bacterial biofilm accelerates SRB MIC of Fe (Xu and Gu, 2014; Dou et al., 2019):

$$\text{Oxidation reaction : } Fe \rightarrow Fe^{2+} + 2e^- \quad (E^{\circ\prime} = -447 \text{ mV}) \quad (3)$$
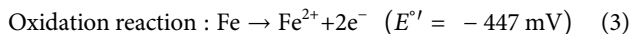
Because elemental iron releases electrons extracellularly and the electrons are used in sulfate reduction inside the cytoplasm of the SRB, extracellular electron transfer (EET) is required. Thus, this kind of MIC is labeled as EET-MIC, which is the result of the demand of electroactive sessile cells for energy. The starved cells are more eager to harvest the extracellular electrons for energy production in order to survive, which can lead to more severe corrosion (Gu and Xu, 2013; Flemming et al., 2016; Liu et al., 2018).

In this work, carbon source starvation was used as a means to vary MIC severity in the study of the MIC impact on the degradation of X80 mechanical properties. Starvation also induced changes in dissolved H_2S and headspace H_2 levels, which were used to study their impact on the degradation as well.

Small X80 square coupons in anaerobic bottles were used for weight loss analysis after the starvation testing. They were also used as working electrodes in electrochemical glass cells for electrochemical tests. The X80 dogbone coupons were used for gas measurements, sessile cell counting, pitting analysis, and tensile testing.

EXPERIMENTAL

Materials

The composition of X80 carbon steel is listed in **Table 1**. Twenty X80 square coupons (with a 1-cm² exposed surface on the top) were used as weight loss samples (12 required) and working electrodes (eight required) in the electrochemical tests. X80 steel was also machined to create dogbone coupons for sulfate-reducing bacterial immersion and subsequent tensile testing. The dimensions of the dogbone coupons were based on the ASTM E8/E8M standard (ASTM-E8/E8M-13a, 2013) (**Figure 1**). Each dogbone coupon was painted with Teflon, except for a middle 2.5-cm section (with four sides unpainted), with a total exposed area slightly over 4 cm². The surfaces of the square coupons for weight losses and electrodes were sequentially polished with 180, 400, and 600 grit abrasive papers. The surfaces of the dogbone coupons were polished to 1,200 grit by the supplier prior to shipping. After painting, all the coupons were cleaned with pure isopropanol and dried under UV light for 20 min. The chemicals used in this work were purchased from Fisher Scientific (Pittsburgh, PA, United States) or Sigma-Aldrich (St Louis, MO, United States).

Culture Media and Inoculum

Desulfovibrio vulgaris (ATCC 7757) was selected in this research as a typical pure-strain SRB. The culture medium was
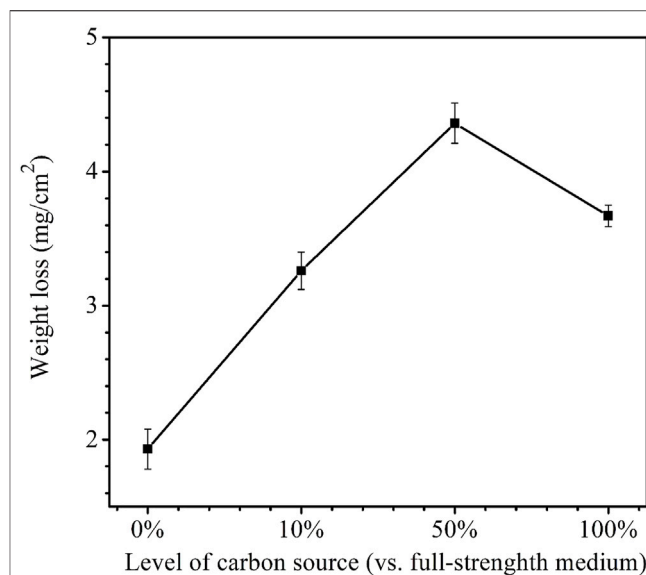

FIGURE 2 | Weight losses after 14-day starvation incubation in 450-ml anaerobic bottles with varied carbon source levels. (Each error bar represents a range of readings from three coupons in the same anaerobic bottle.).

an ATCC 1249 medium (composition in **Table 2**), which is a modified Baar's medium for sulfate reducers. The initial pH in each anaerobic bottle prior to each inoculation was adjusted to 7 by using HCl or NaOH solution as required before sterilization in an autoclave at 121°C for 40 min. After autoclaving, the SRB culture media were deoxygenated using filter-sterilized N_2 sparging for more than 45 min. About 100 ppm L-cysteine was then added to the culture media as an oxygen scavenger to reduce dissolved oxygen further and to mitigate possible oxygen leakage. All incubations were carried out at 37°C anaerobically. About 200 mL of the deoxygenated sterilized culture medium and 2 ml of SRB seed culture were put into each 450-ml anaerobic bottle for 3-day SRB pre-growth in the full-strength ATCC 1249 medium. Each bottle contained three square coupons (at the bottom) or one dogbone coupon (leaning on the wall at a 30° angle with the bottom). The dogbone was not pulled or stressed during incubation. This was compatible with the field situation in which a support beam normally under no load or of a small load is corroded by SRB. When a large load (e.g., a heavy truck on a bridge) finally comes, the beam fails. After the 3-day pre-growth, the square coupons, including the working electrode coupons (already in the epoxy resin), and the dogbone coupons were covered with mature biofilms. They were transferred into other 450-ml anaerobic bottles with fresh culture media containing different levels of the carbon source (0, 10, 50, and 100% vs the carbon source in the standard ATCC 1249 medium) for an additional 14-day carbon starvation incubation. Both lactate and citrate were adjusted to vary the carbon source levels in the ATCC 1249 medium, although only lactate is known to be utilized by *D. vulgaris* as a carbon source.
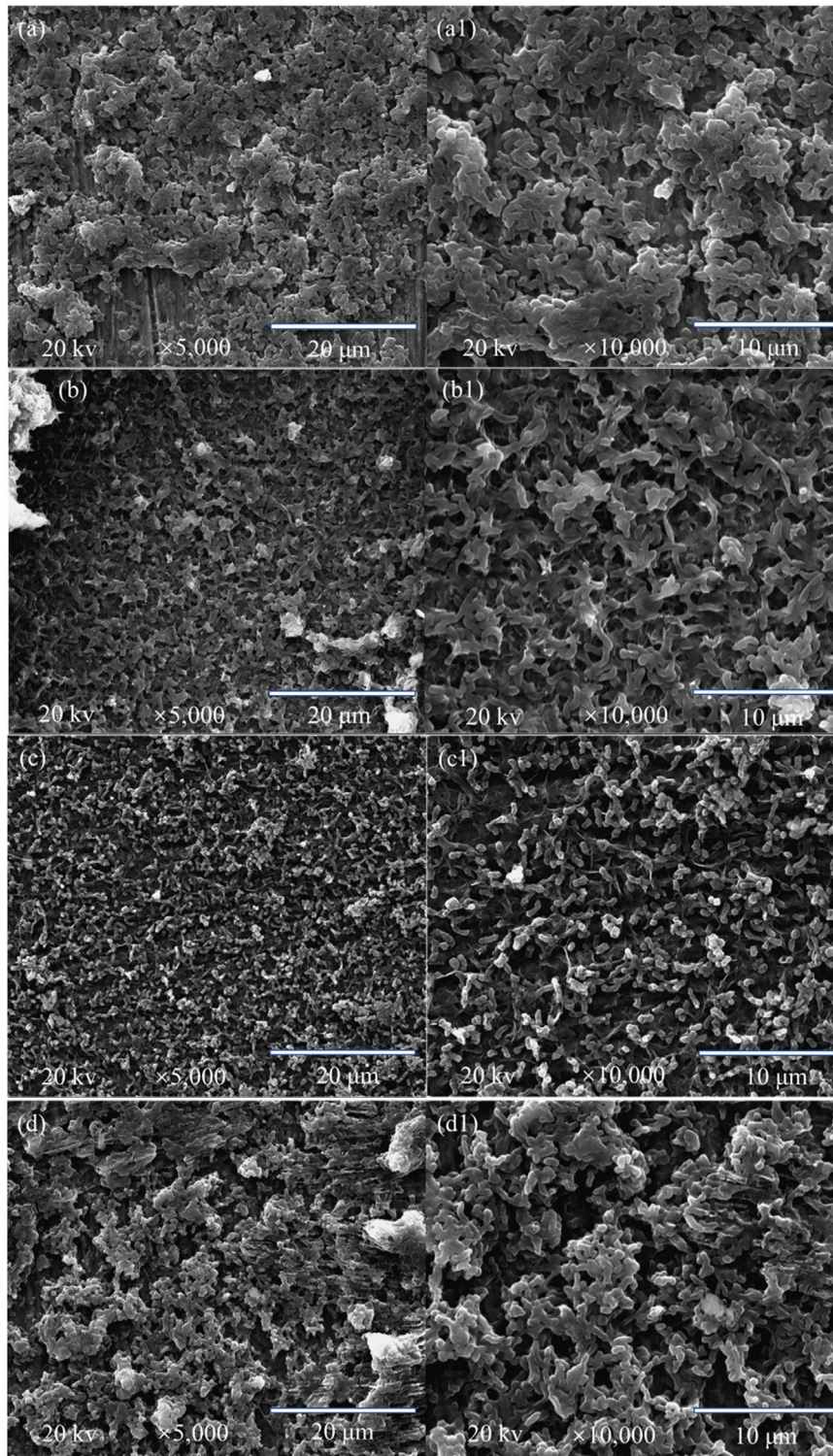
FIGURE 3 | SEM images of the square coupon surfaces after 14-day starvation incubation in anaerobic vials with 200 ml of *D. vulgaris* broth, 250 ml of headspace, and carbon source levels of 0% **(a,a1)**, 10% **(b,b1)**, 50% **(c,c1)**, and 100% **(d,d1)**.

Weight Loss

In this study, because the dogbone coupons were too heavy to obtain the milligram weight losses accurately, small X80 coupons with a 1-cm^2 exposed top surface were used for the weight loss analysis. After the starvation incubation, the square coupons were cleaned with fresh Clarke's solution to remove biofilms and
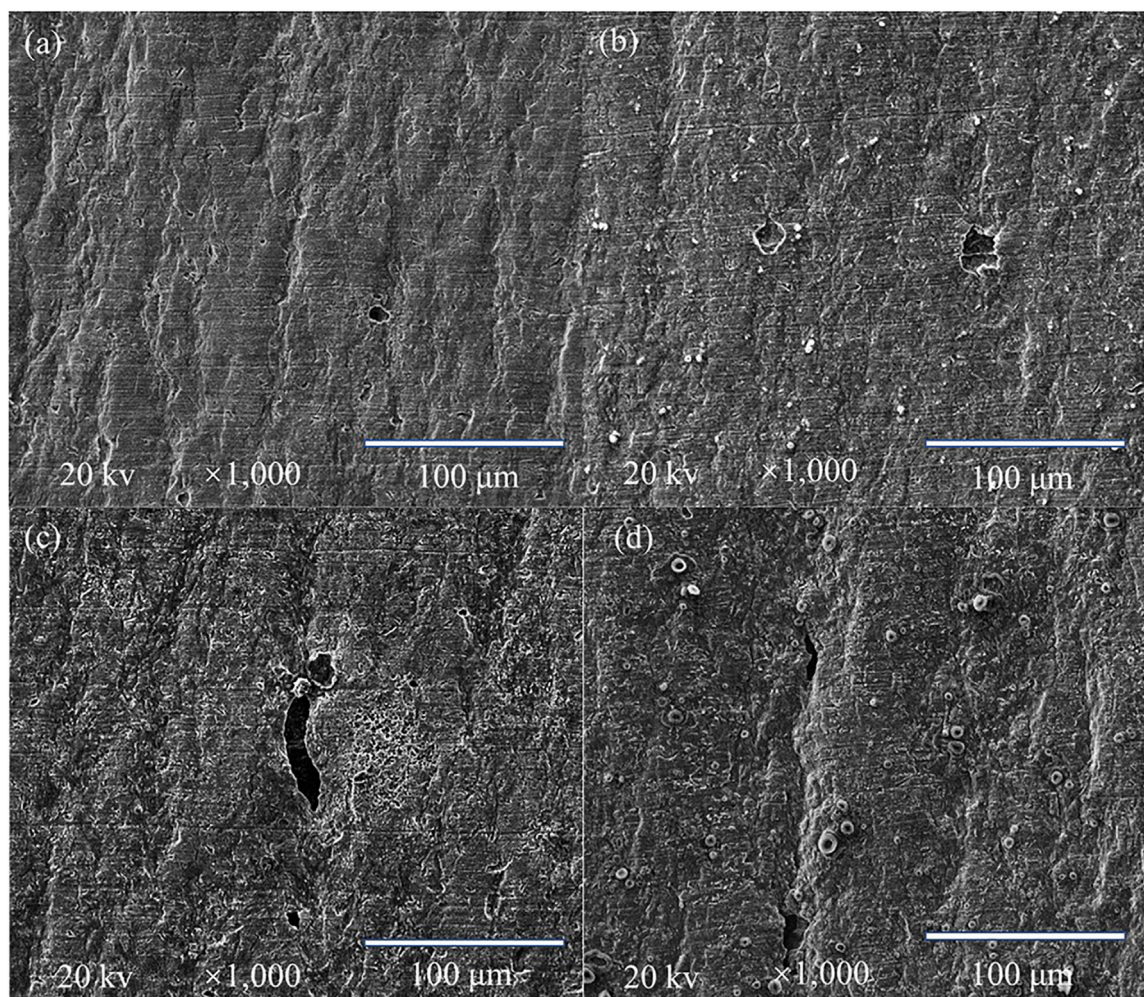
FIGURE 4 | SEM images for the X80 square coupons (with corrosion products removed) after 14-day starvation incubation in an anaerobic vial with 200 ml of *D. vulgaris* broth, 250 ml of headspace, and carbon source levels of 0% **(A)**, 10% **(B)**, 50% **(C)**, and 100% **(D)**.

corrosion products before weighing to obtain the weight loss data. Each weight loss data point was the average of three replicate coupons from the same anaerobic bottle.

Surface and Biofilm Analysis

After 14 days of starvation incubation, the X80 square coupons were retrieved. A scanning electron microscope (SEM) (FEI Quanta 250, Hillsboro, OR, United States) was used to observe the biofilm morphology on the square coupon surfaces. Before biofilm observation, the coupons were first cleaned with pH 7.40 phosphate-buffered saline (PBS) solution for 15 s, and then soaked in 2.5% (w/w) glutaraldehyde solution for 8 h at 10°C to fix the biofilm. Afterward, the coupons were dehydrated with 50% (v/v), 70%, 80%, 90%, and 95% ethanol sequentially for 10 min at each concentration and 100% ethanol for 30 min at the end (Cui et al., 2020). Then, the coupon surfaces were sputter coated with Au to provide surface conductivity. Subsequently, the same coupons were cleaned using Clarke's solution to remove

biofilms and corrosion products before pit image analysis under the SEM and finally used for weight loss measurements.

Electrochemical Measurements

A VersaSTAT 3 potentiostat from Princeton Applied Research (Oak Ridge, TN, United States) was used to measure the electrochemical responses of the X80 working electrodes for varied carbon source levels in *D. vulgaris* broths. Each glass cell contained 200 ml of culture medium with a varied carbon source (0, 10, 50, and 100%) and 250 ml of headspace. It was inoculated with 2 ml of SRB seed culture before 3-day pre-growth incubation at 37°C. A saturated calomel electrode was used as the reference electrode, and a platinum plate (10 mm × 10 mm × 1 mm) was used as the counter electrode. Open circuit potential (OCP), linear polarization resistance (LPR), and potentiodynamic polarization analyses were performed. The LPR was scanned at a rate of 0.1667 mV/s in the range of −10 mV to +10 mV vs the OCP. Electrochemical impedance
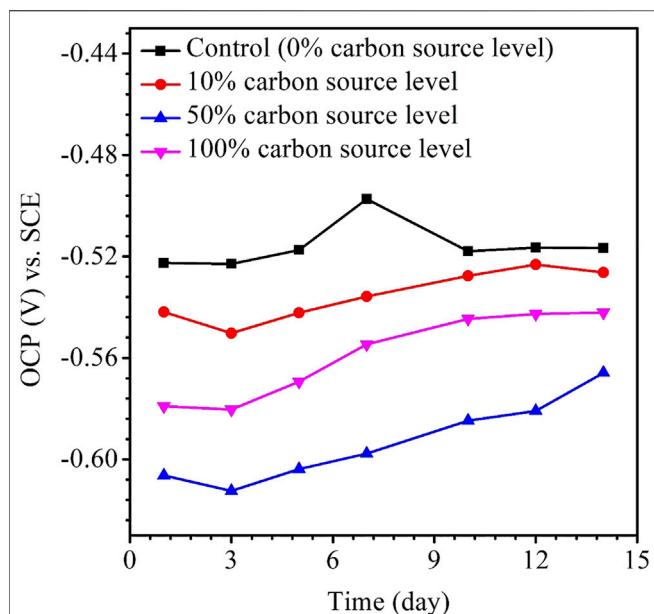
FIGURE 5 | Variations of the OCP vs. time for X80 during 14-days starvation incubation.
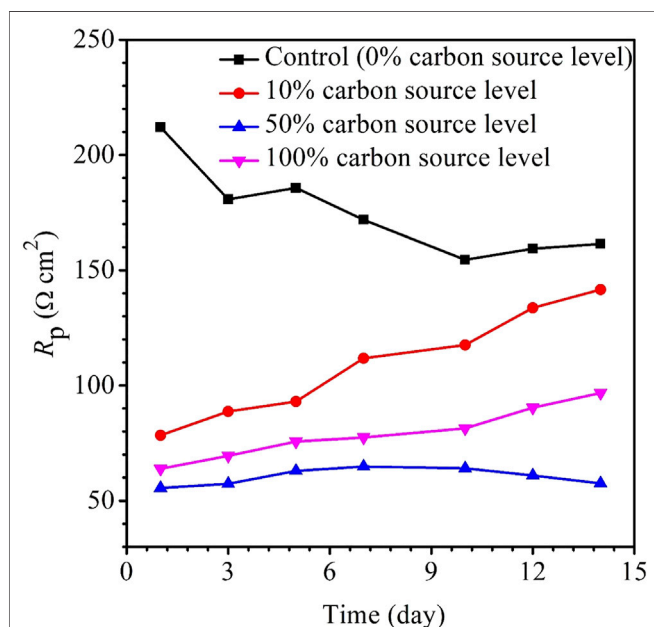

FIGURE 6 | Variations of R_p vs time for X80 during 14-days starvation incubation.

electrode in a different glass cell at a rate of 0.1667 mV/s. The corrosion potential (E_{corr}), corrosion current density (i_{corr}), and anodic and cathodic Tafel slopes (β_a and β_c) were determined from the Tafel analysis of the polarization curves.

Gas Measurements, Sessile Cell Counts, Pit Depths, and Tensile Testing

After the starvation test, the concentrations of H_2S and H_2, as well as the total pressure in the headspace of each anaerobic bottle containing one dogbone coupon were measured using a portable H_2S sensor (GAXT-H-DL, BW Technologies, Calgary, Alberta, Canada), a portable H_2 sensor (BH-90A, Forensics Detectors, Palos Verdes Peninsula, CA, United States), and a digital manometer (Xplorer GLX-PS-2002, PASCO scientific, Roseville, CA, United States), respectively. The H_2S sensor has an upper detection limit of 100 ppm (v/v). If a headspace sample had a high concentration, dilution was required. A 125-ml bottle sealed with 1 atm air was injected with 10 ml of headspace gas for 12.5× dilution. After mixing, a syringe was used to flush and flood the sensor's sample port with 40 ml of the headspace gas before taking a meter reading.

The pH value of each SRB broth was measured for all dogbone bottles after the starvation incubation. After the starvation incubation, the dogbone coupons were taken out and rinsed three times in PBS of pH 7.40 to remove loosely attached planktonic cells and culture medium. Sessile cells on each dogbone coupon's exposed section were removed using a small disposable brush into 10 ml of PBS solution in a disposable plastic weighing dish. Then, the brush, the coupon, and 10 ml PBS solution were vortexed together in a 50-ml conical tube for 30 s.

After the sessile cell counting using a hemocytometer had been carried out (Li et al., 2015), each dogbone coupon was cleaned using Clarke's solution before it was scanned using an Infinite Focus Microscope (IFM) (Model ALC13, Alicona Imaging GmbH, Graz, Austria) to obtain the pit depth profiles.

Finally, all the dogbone coupons after SRB incubation and a fresh X80 dogbone coupon were subjected to tensile testing on an electromechanical universal testing machine (E44.304, MTS system, MN, United States) to obtain stress–strain curves. The strain rate used in the testing was 0.004 s^{-1}.

RESULTS AND DISCUSSION

Weight Loss Using Square Coupons

After the 14-day carbon starvation incubation, the coupon weight losses for the carbon source levels of 0, 10, 50, and 100% were obtained. They are shown in **Figure 2**. The highest weight loss was 4.4 mg/cm^2 for 50% carbon source and the lowest was 1.9 mg/cm^2 for 0% carbon source. The weight loss for 10% carbon source 3.3 mg/cm^2 and weight loss for 100% carbon source 3.7 mg/cm^2 were close. It is to be noted that 0% carbon source had the lowest weight loss instead of the highest. This was because the extreme starvation had led to much loss of sessile cells (Xu and Gu, 2014; Dou et al., 2019).

spectroscopy (EIS) was performed at the OCP by applying a sinusoidal signal of 10 mV (amplitude) in the frequency ranging from 10^4 to 10^{-2} Hz. Potentiodynamic polarization curves were scanned at the end of the 14-day starvation incubation from the OCP to −200 mV vs. the OCP using one working electrode, and from the OCP to +200 mV vs. the OCP using a replicate working
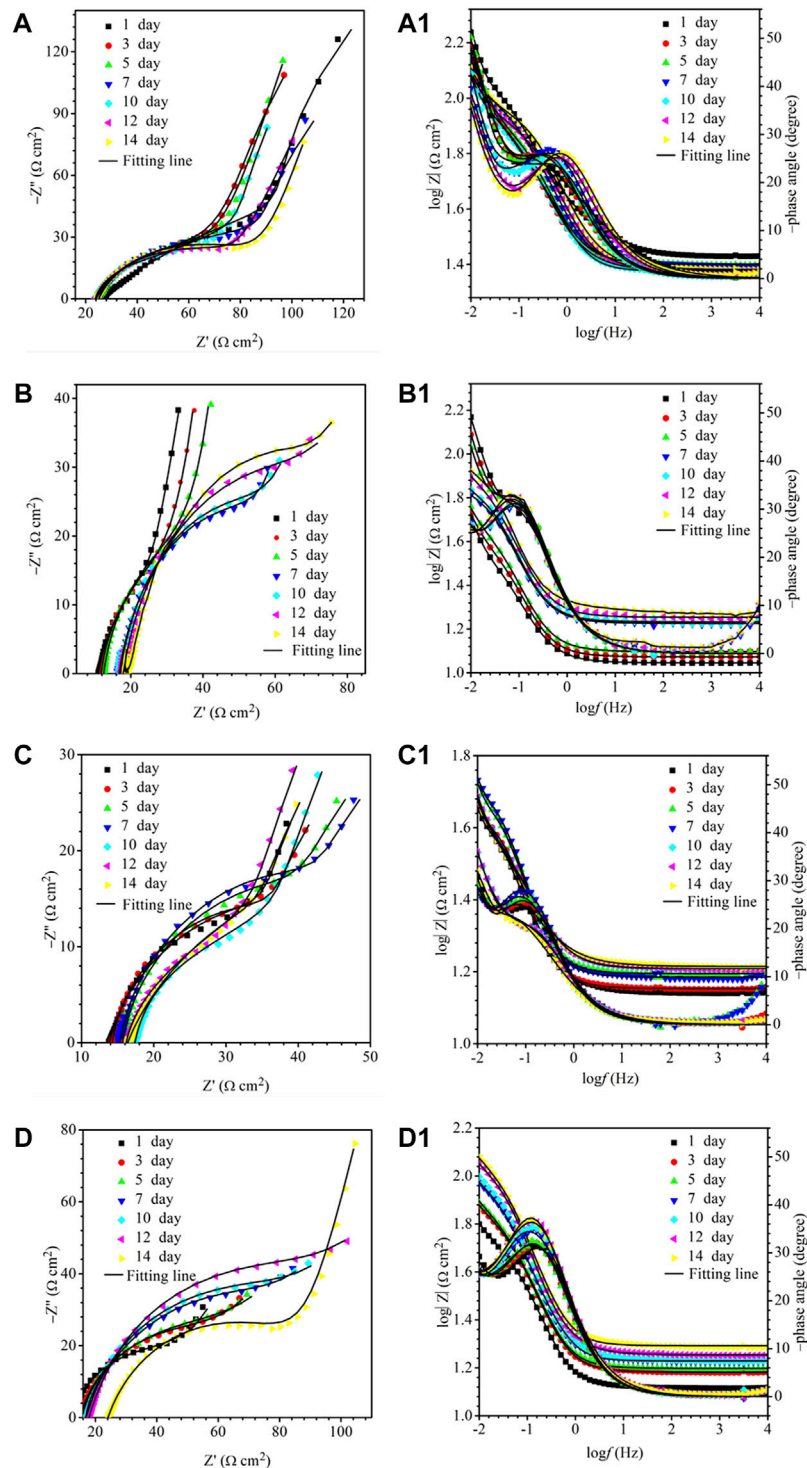
FIGURE 7 | Nyquist and Bode plots for X80 during 14-days incubation in an anaerobic vial with 200 ml of *D. vulgaris* broth, 250 ml of headspace, and carbon source levels of 0% **(a,a1)**, 10% **(b,b1)**, 50% **(c,c1)**, and 100% **(d,d1)**.

Surface and Biofilm Analyses Using Square Coupons

The SEM images in **Figure 3** depict the surface morphologies of the *D. vulgaris* biofilms under different carbon sources after 14-day carbon starvation incubation. The amount of sessile cells on their surfaces were increasing with increasing carbon source levels, from 0% carbon source level to 100% carbon source level as expected. The SEM images in **Figure 4** are consistent

TABLE 3 | Electrochemical parameters obtained from fitting EIS spectra in **Figure 7**.
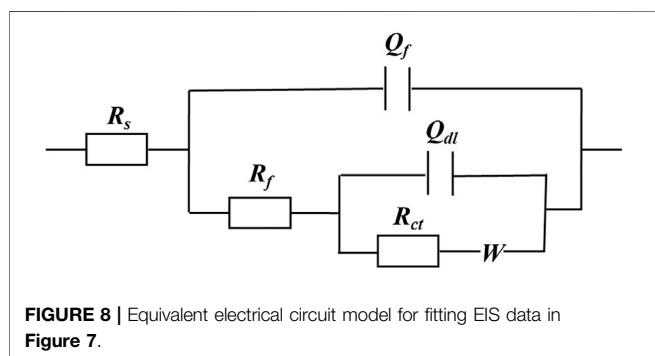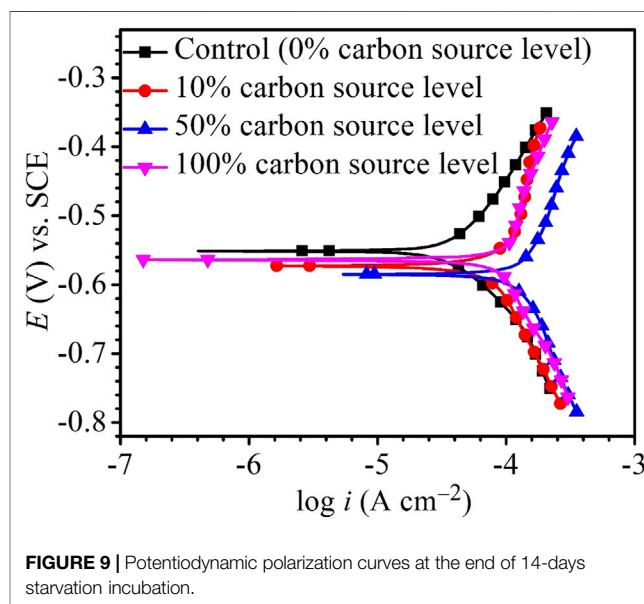
Carbon source level	t (d)	R_s (Ω cm^2)	Q_{dl} (Ω^{-1} cm^{-2} s^n)	n_1	R_f (Ω cm^2)	Q_{dl} (Ω^{-1} cm^{-2} s^n)	n_2	R_{ct} (Ω cm^2)	W-R (Ω cm^2)	W-T (s)	W-P
0%	1	26.7	1.09×10^{-2}	0.63	31.2	1.03×10^{-2}	0.44	182	80.6	3.43	0.63
	3	23.8	1.61×10^{-2}	0.73	74.5	7.91×10^{-2}	0.96	110	1.26×10^3	68.4	0.64
	5	25.1	1.38×10^{-2}	0.79	65.5	7.50×10^{-2}	0.90	121	309	3.51	0.35
	7	25.1	9.56×10^{-3}	0.85	44.9	3.54×10^{-2}	0.56	131	38.4	2.21	0.61
	10	23.7	1.03×10^{-2}	0.87	33.9	4.10×10^{-2}	0.63	112	76.2	4.79	0.58
	12	23.9	9.62×10^{-3}	0.78	63.5	1.01×10^{-1}	0.78	82.1	215	2.74	0.63
	14	24.1	8.41×10^{-3}	0.76	73.9	1.26×10^{-1}	0.84	79.2	145	1.01	0.71
10%	1	11.1	8.43×10^{-2}	0.83	28.8	1.51×10^{-1}	0.80	49.1	101	3.93	0.63
	3	11.2	7.82×10^{-2}	0.85	36.7	2.52×10^{-1}	0.98	53.1	148	14.4	0.43
	5	12.5	7.30×10^{-2}	0.84	44.1	2.51×10^{-1}	0.97	45.9	106	7.91	0.42
	7	16.8	6.05×10^{-2}	0.83	53.1	5.41×10^{-1}	0.95	60.6	108	8.02	0.55
	10	17.1	5.81×10^{-2}	0.84	57.7	3.77×10^{-1}	0.82	63.9	182	8.99	0.64
	12	17.9	5.21×10^{-2}	0.83	61.2	1.48×10^{-1}	0.54	76.8	198	14.2	0.62
	14	18.9	4.97×10^{-2}	0.81	68.4	1.04×10^{-1}	0.43	79.8	195	14.3	0.65
50%	1	13.9	7.20×10^{-2}	0.83	10.8	4.60×10^{-2}	0.30	45.1	56.9	11.4	0.63
	3	14.2	7.04×10^{-2}	0.88	12.2	4.60×10^{-2}	0.28	42.3	48.3	9.81	0.63
	5	15.7	6.91×10^{-2}	0.88	15.7	4.91×10^{-2}	0.30	45.7	71.9	11.2	0.62
	7	15.3	6.63×10^{-2}	0.88	17.3	4.51×10^{-2}	0.26	48.9	78.6	12.2	0.63
	10	17.4	5.57×10^{-2}	0.82	23.3	2.05×10^{-1}	0.73	35.5	63.9	4.19	0.55
	12	16.2	7.07×10^{-2}	0.78	27.3	2.92×10^{-1}	0.96	32.8	59.8	10.6	0.42
	14	16.4	8.47×10^{-2}	0.70	28.3	9.06×10^{-2}	0.52	33.5	37.8	6.03	0.66
100%	1	13.1	3.80×10^{-2}	0.90	20.5	4.19×10^{-2}	0.43	43.5	224	96.2	0.73
	3	15.2	3.56×10^{-2}	0.87	25.5	2.56×10^{-2}	0.50	44.9	241	212	0.72
	5	15.8	3.41×10^{-2}	0.89	29.3	4.15×10^{-2}	0.63	47.3	364	359	0.76
	7	16.9	2.71×10^{-2}	0.93	31.5	3.62×10^{-2}	0.83	49.1	323	415	0.70
	10	17.0	3.25×10^{-2}	0.80	37.3	3.20×10^{-3}	0.99	50.7	405	592	0.71
	12	17.9	2.74×10^{-2}	0.84	44.8	9.72×10^{-3}	0.96	51.1	376	442	0.69
	14	19.6	9.03×10^{-1}	0.90	50.8	2.74×10^{-2}	0.80	49.1	425	552	0.63

FIGURE 8 | Equivalent electrical circuit model for fitting EIS data in **Figure 7**.

FIGURE 9 | Potentiodynamic polarization curves at the end of 14-days starvation incubation.

with the weight loss findings that 50% carbon source level caused the most severe corrosion and 0% the least.

Electrochemical Tests Using Square Coupons

The variations of the OCP during the 14-day carbon starvation are shown in **Figure 5**. A lower OCP indicates a higher tendency for the working electrode to lose electrons (i.e., undergoing oxidation) or be corroded. During the starvation period, 50% carbon source had the lowest OCP and 0% the highest, which is consistent with the weight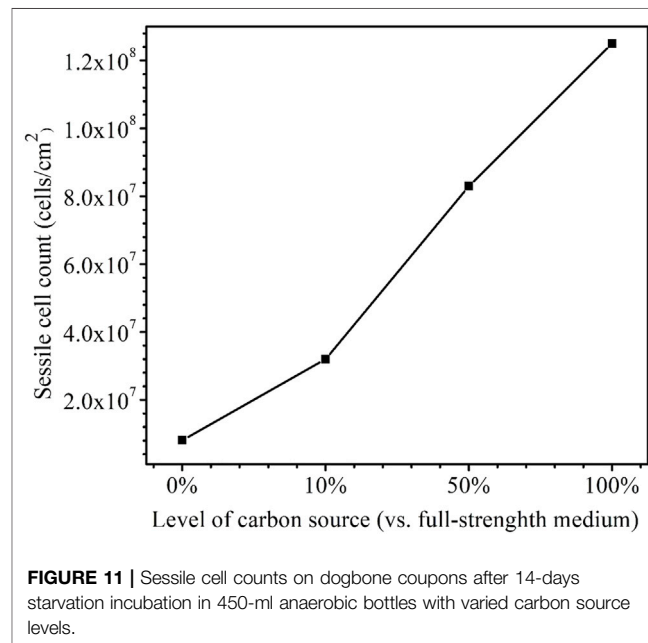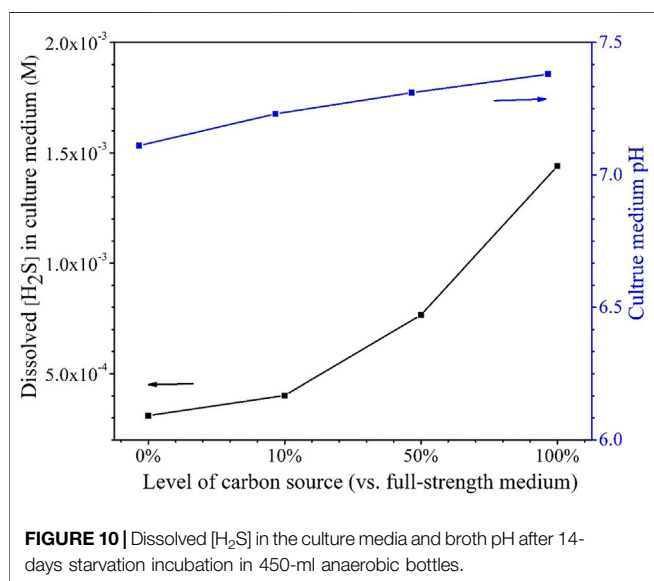 loss trend. In MIC, sometimes, the OCP trends are not always correct because the OCP only indicates to a tendency without factoring in the actual corrosion speed. The kinetic electrochemical data on corrosion

TABLE 4 | Fitted electrochemical parameters from Tafel analysis of **Figure 9**.

Carbon source level (%)	i_{corr} (μA/cm²)	E_{corr} (mV) vs SCE	β_a (mV/dec)	β_c (mV/dec)
0	41	−561	294	−187
10	84	−564	469	−348
50	145	−599	604	−525
100	98	−616	945	−364

TABLE 5 | Headspace gas concentrations and total pressure as well as calculated [H₂S] after 14-day carbon starvation incubation in dogbone bottles.

Carbon source level (vs full-strength medium	(%) Total pressure in headspace (bar)	H_2 concentration in headspace (10^3 ppm) (v/v)	H_2S concentration in headspace (10^3 ppm) (v/v)	Dissolved [H_2S] in liquid phase (10^{-4} M)
0	1.03	0.75	4.08	3.10
10	1.07	1.16	5.08	4.01
50	1.16	1.95	9.00	7.66
100	1.55	2.50	12.6	14.4

FIGURE 10 | Dissolved [H₂S] in the culture media and broth pH after 14-days starvation incubation in 450-ml anaerobic bottles.

FIGURE 11 | Sessile cell counts on dogbone coupons after 14-days starvation incubation in 450-ml anaerobic bottles with varied carbon source levels.

resistance or corrosion current are more reliable (Jia et al., 2019). In corrosion kinetics, R_p is inversely proportional to the corrosion rate. **Figure 6** shows that the R_p for the 50% carbon source level is the lowest, corresponding to the highest corrosion rate, followed by 100, 10, and 0% carbon source levels. The $1/R_p$ here is consistent with the weight loss trend.

The EIS Nyquist and Bode plots of the X80 square coupons for different carbon source levels on different days during the 14-day starvation incubation are shown in **Figure 7**. The corresponding fitted parameters are listed in **Table 3**. The Nyquist plots of the square coupons indicate a capacitive behavior and a diffusion phenomenon. The equivalent circuit model is shown in **Figure 8**, in which R_s is solution resistance, R_f and Q_f are the resistance and constant-phase element of the biofilm, respectively. R_{ct} is the

charge-transfer resistance, Q_{dl} the constant-phase element of the electric double layer, and W is the Warburg element describing the diffusion process. The presence of W in **Figures 7**, **8** and **Table 3** was caused by the mass transfer resistance effect exerted by the biofilm and corrosion product film on the X80 working electrode (Yin et al., 2018). The impedance spectra for different carbon source levels fitted well with the two-time constant circuit model. The 50% carbon source level had the smallest diameters of the semi-circles in the Nyquist plots (**Figure 7**) and the smallest value of ($R_{ct} + R_b$) (**Table 3**), which means that the 50% carbon source level exhibited the highest corrosion rate (Dou et al., 2019). The EIS results are consistent with the LPR results (**Figure 6**), supporting the weight loss trend (**Figure 2**).
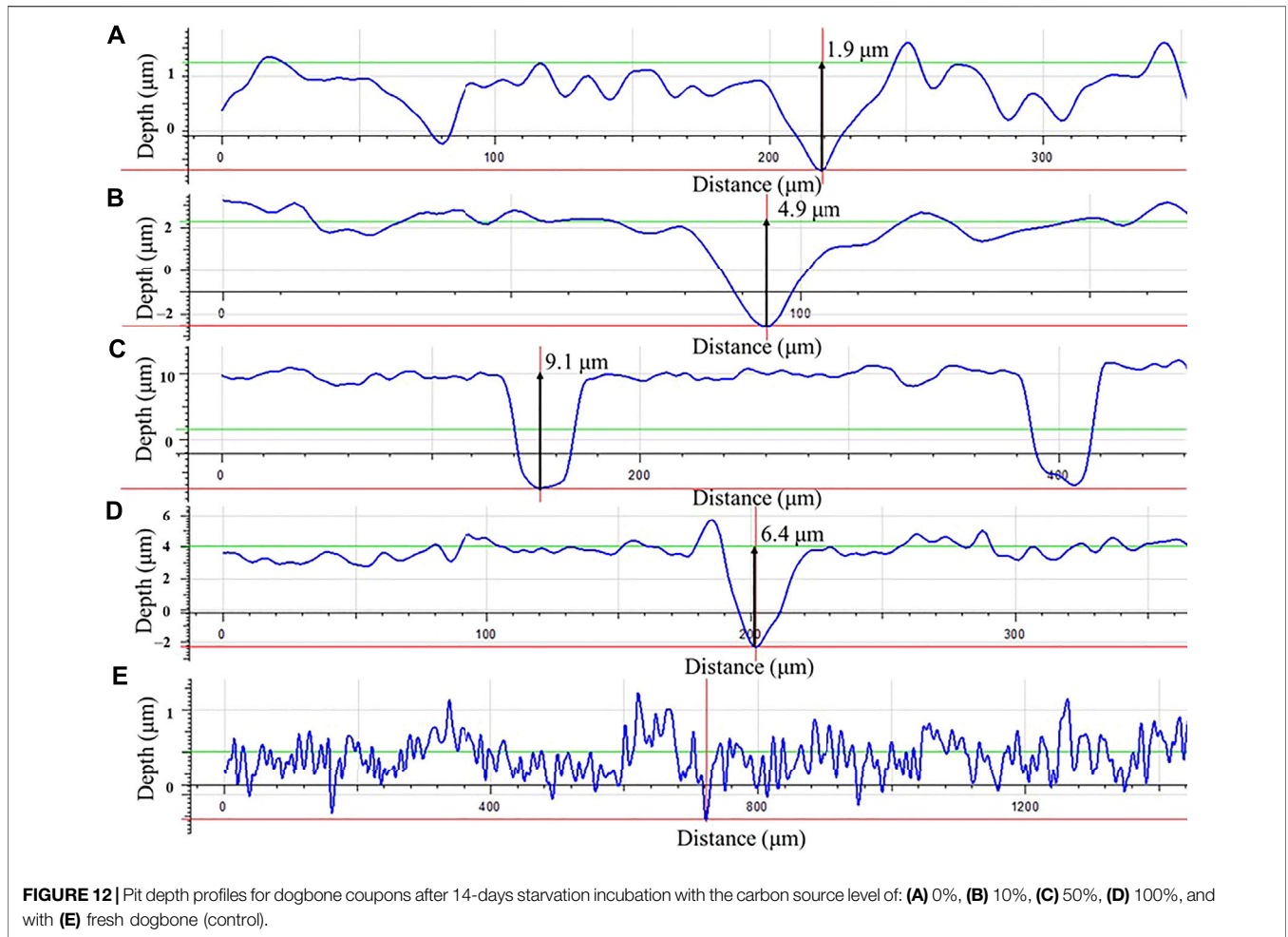
FIGURE 12 | Pit depth profiles for dogbone coupons after 14-days starvation incubation with the carbon source level of: **(A)** 0%, **(B)** 10%, **(C)** 50%, **(D)** 100%, and with **(E)** fresh dogbone (control).
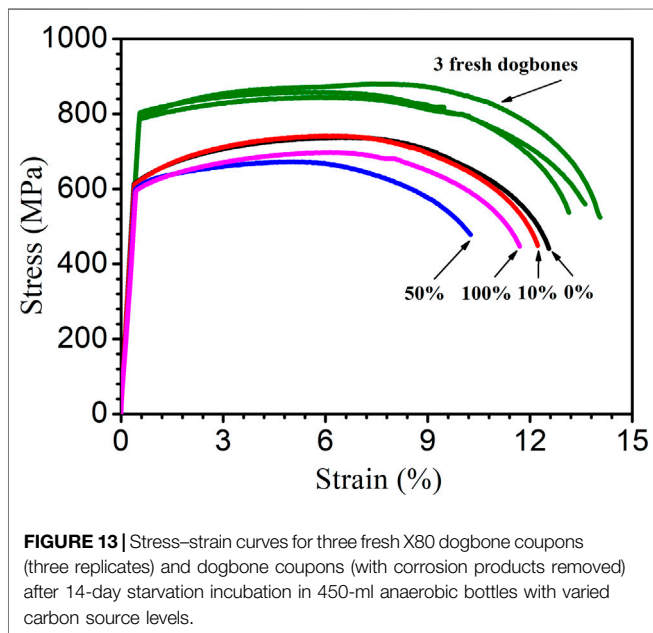

FIGURE 13 | Stress–strain curves for three fresh X80 dogbone coupons (three replicates) and dogbone coupons (with corrosion products removed) after 14-day starvation incubation in 450-ml anaerobic bottles with varied carbon source levels.

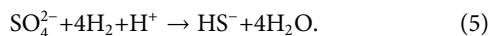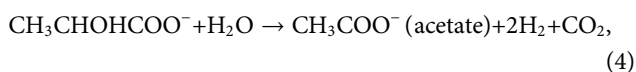**TABLE 6 |** Ultimate tensile strength and ultimate tensile strain data from **Figure 13**.

Carbon source level	Ultimate tensile strength (MPa) (and loss)	Ultimate tensile strain (%) (and loss)
(No immersion)	860 ± 17.6 (control)	13.6 ± 0.5% (control)
0%	736 (14% loss)	12.7% (7% loss)
10%	741 (14% loss)	12.2% (10% loss)
50%	672 (22% loss)	10.3% (24% loss)
100%	697 (19% loss)	11.7% (14% loss)

The Tafel plots are shown in **Figure 9**. Because potentiodynamic polarization scans use a large voltage range, they may alter the surface of the working electrode. Thus, Tafel scans are usually performed only once at the end. In this work, they were performed at the end of the 14-day starvation period after all the other electrochemical measurements. The fitted Tafel parameters are listed in **Table 4**. The i_{corr} data here are consistent with the weight loss trend showing 50% carbon source having the highest value (145 μA/cm^2), followed by 100% carbon source (98 μA/cm^2), 10% carbon source (84 μA/cm^2), and 0% carbon source

(41 μA/cm^2). The i_{corr} trend here is consistent with the weight loss trend. This work showed that LPR, EIS, and Tafel scans, all confirmed the weight loss trend, suggesting that the electrochemical methods are valuable in MIC studies. Furthermore, the weight loss only reflects the cumulative corrosion outcome, but nondestructive LPR and EIS can provide transient corrosion behaviors.

Dogbone Bottles: H$_2$ Concentration, H$_2$S Concentration, Total Pressure

Table 5 shows that a higher carbon source level led to a higher concentration of H$_2$. This H$_2$ trend is reasonable because it is known that *D. vulgaris* produces H$_2$ during lactate oxidation, and later it consumes H$_2$ when there is a shortage of organic carbon (Wang et al., 2020).

$$\text{CH}_3\text{CHOHCOO}^- + \text{H}_2\text{O} \rightarrow \text{CH}_3\text{COO}^- \text{ (acetate)} + 2\text{H}_2 + \text{CO}_2, \tag{4}$$

$$\text{SO}_4^{2-} + 4\text{H}_2 + \text{H}^+ \rightarrow \text{HS}^- + 4\text{H}_2\text{O}. \tag{5}$$

HS$^-$ can absorb one proton to become H$_2$S or lose one proton to become S^{2-} as shown below (Gu and Xu, 2013):

$$\text{HS}^- + \text{H}^+ \rightarrow \text{H}_2\text{S}, \tag{6}$$

$$\text{HS}^- \rightarrow \text{H}^+ + \text{S}^{2-}. \tag{7}$$

The H$_2$S data in **Table 5** indicate that better SRB growth (as a result of a higher carbon source level) produced more H$_2$S from sulfate reduction. The dissolved H$_2$S concentrations in the liquid phases were estimated based on H$_2$S equilibrium at 37°C (Ning et al., 2014). The dissolved [H$_2$S] in the culture medium data was plotted together with broth pH data at the end of the 14-day starvation incubation as shown in **Figure 10**. **Figure 10** clearly indicates that a higher dissolved H$_2$S concentration corresponds to a higher pH. This contradicts the conventional thinking of more H$_2$S in a system for more acidic liquid pH (lower pH). This is because in abiotic H$_2$S corrosion testing, externally introduced H$_2$S acidifies the liquid phase due to H$_2$S dissociation, which releases protons. However, in the SRB broth, H$_2$S is as a reservoir of H$^+$, but its H$^+$ originally comes from the broth itself rather than being externally introduced. Thus, it is not rational to argue for acidification by biogenic H$_2$S in the SRB system. More dissolved H$_2$S in the SRB system results in a higher and not a lower pH.

It is known that sulfate respiration does not normally change scalar and vectorial protons (Peck, 1993). On the contrary, better SRB growth allows more H$_2$S to escape to the headspace, thus taking away more proton from the broth. This is why **Figure 10** shows a higher carbon source level leading to a higher broth pH (7.38 for 100% carbon source, 7.31 for 50% carbon source, 7.23 for 10% carbon source, and 7.11 for 0% carbon source). In fact, SRB are used to increase the pH of acid mine drainage for exactly the same reason as demonstrated here (Bai et al., 2013). The above 7.00 pH values in **Figure 10** also suggest that acid attack and H$_2$S

attack were not important contributors to the MIC in this work (Wang et al., 2020).

Sessile Cell Counts on Dogbone Coupons

After the 14-day starvation incubation, the sessile cell count was found to be higher for a larger carbon source level as was expected (**Figure 11**). The cell counts on the dogbone coupons in the bottles with the carbon source levels of 0, 10, 50, and 100% were 8.1×10^6, 3.2×10^7, 8.3×10^7, and 1.3×10^8 cells/cm^2, respectively. The 0% carbon source bottle had the lowest sessile cell count due to extreme starvation (Dou et al., 2019). The sessile cell counts on the X80 dogbone coupons here are consistent with the SEM biofilm images on the X80 square coupons.

Pit Depths on Dogbone Coupons

Morphologies of MIC pits on the dogbone coupons after the 14-day carbon starvation incubation with biofilms and with corrosion products removed were examined under the IFM before tensile testing (**Figure 12**). The maximum pit depth was the highest for 50% carbon source (9.1 μm) followed by 100% carbon source (6.4 μm), 10% carbon source (4.9 μm), and 0% carbon source (1.9 μm). The pit depth trend here is consistent with the weight loss trend.

Tensile Testing Using Dogbone Coupons

Figure 13 shows the stress–strain curves of the dogbone coupons after the 14-day starvation incubation. Compared with the fresh X80 dogbone's ultimate strength of 879 MPa, all the biotic dogbone coupons had a lower ultimate tensile strength and ultimate tensile strain. **Table 6** shows a summary. It indicates that the trend of the degradation of the ultimate tensile strain followed the trend of MIC severity (in terms of weight loss and pit depth) and followed the following sequence (more to less): 50, 100, 10, and 0% carbon source levels. The degradation of the ultimate strength followed the same general trend (but with 10 and 0% having practically the same value). A lower ultimate tensile strain means a more brittle metal. Thus, the tensile strain data indicated that SRB MIC made X80 more brittle in addition to weakening its mechanical strength.

The 50% carbon source led to the highest reductions in both ultimate tensile strength (22% loss) and ultimate tensile strain (24% loss) compared with the fresh dogbone data. In this work, 50% carbon source caused the biggest MIC damages in terms of weight loss and pitting depth. As a result, it led to the most severe degradation of X80 mechanical properties. This trend could not be attributed to H$_2$ or H$_2$S because 50% source did not have the highest H$_2$ or H$_2$S level. In abiotic H$_2$S studies, externally introduced H$_2$S acidifies a liquid, which causes corrosion. But it was not the case in this study with biogenic H$_2$S production, which does not acidify the liquid phase. Thus, it was not surprising that the highest dissolved H$_2$S concentration (100% carbon source) did not result in the highest losses to ultimate strength and ultimate tensile strain.

CONCLUSIONS

(1) The weight loss data using square coupons indicated that 50% carbon source levels resulted in the highest weight loss. This was because 50% carbon had the combination of carbon starvation without suffering too much sessile cell loss. The weight loss trend was supported by the pit depth trend.

(2) The electrochemical results, including LPR, EIS, and Tafel scans, all supported the weight loss trend, confirming that the 50% carbon source level caused the most severe MIC.

(3) The SEM biofilm results agreed with the sessile cell count trend.

(4) The H_2S, H_2, and sessile cell count data for dogbone coupons were consistent in supporting the higher carbon source levels for better growth, exhibiting higher biogenic H_2S and H_2 concentrations.

(5) The tensile test results for the biotic coupons and the fresh X80 dogbone showed that more severe MIC led to larger degradations of ultimate tensile strain and ultimate tensile strength. The 50% carbon source led to the highest reductions in both ultimate tensile strength (22% loss vs fresh dogbone) and ultimate tensile strain (24% loss).

(6) A higher dissolved H_2S concentration at a nonacidic pH in this work did not result in higher losses in ultimate strength and ultimate tensile strain because it did not provide higher weight loss and pit depth.

REFERENCES

Abedi, S. S., Abdolmaleki, A., and Adibi, N. (2007). Failure Analysis of SCC and SRB Induced Cracking of a Transmission Oil Products Pipeline. *Eng. Fail. Anal.* 14, 250–261. doi:10.1016/j.engfailanal.2005.07.024

Al-Nabulsi, K. M., Al-Abbas, F. M., Rizk, T. Y., and Salameh, A. E. M. (2015). Microbiologically Assisted Stress Corrosion Cracking in the Presence of Nitrate Reducing Bacteria. *Eng. Fail. Anal.* 58, 165–172. doi:10.1016/j.engfailanal.2015.08.003

AlAbbas, F. M., Williamson, C., Bhola, S. M., Spear, J. R., Olson, D. L., Mishra, B., et al. (2013). Influence of Sulfate Reducing Bacterial Biofilm on Corrosion Behavior of low-alloy, High-Strength Steel (API-5L X80). *Int. Biodeterioration Biodegradation* 78, 34–42. doi:10.1016/j.ibiod.2012.10.014

ASTM-E8/E8M-13a (2013). *Standard Test Methods for Tension Testing of Metallic Materials*. West Conshohocken, PA: ASTM International.

Bai, H., Kang, Y., Quan, H., Han, Y., Sun, J., and Feng, Y. (2013). Treatment of Acid Mine Drainage by Sulfate Reducing Bacteria with Iron in Bench Scale Runs. *Bioresour. Technology* 128, 818–822. doi:10.1016/j.biortech.2012.10.070

Biswas, S., and Bose, P. (2005). Zero-valent Iron-Assisted Autotrophic Denitrification. *J. Environ. Eng.* 131, 1212–1220. doi:10.1061/(ASCE)0733-937210.1061/(asce)0733-9372(2005)131:8(1212)

Cui, L. Y., Liu, Z. Y., Xu, D. K., Hu, P., Shao, J. M., Du, C. W., et al. (2020). The Study of Microbiologically Influenced Corrosion of 2205 Duplex Stainless Steel Based on High-Resolution Characterization. *Corrosion Sci.* 174, 108842. doi:10.1016/j.corsci.2020.108842

Dannenberg, S., Kroder, M., Dilling, W., and Cypionka, H. (1992). Oxidation of H2, Organic Compounds and Inorganic Sulfur Compounds Coupled to Reduction of O2 or Nitrate by Sulfate-Reducing Bacteria. *Arch. Microbiol.* 158, 93–99. doi:10.1007/BF00245211

Dou, W., Liu, J., Cai, W., Wang, D., Jia, R., Chen, S., et al. (2019). Electrochemical Investigation of Increased Carbon Steel Corrosion via Extracellular Electron Transfer by a Sulfate Reducing Bacterium under Carbon Source Starvation. *Corrosion Sci.* 150, 258–267. doi:10.1016/j.corsci.2019.02.005

Flemming, H.-C., Wingender, J., Szewzyk, U., Steinberg, P., Rice, S. A., and Kjelleberg, S. (2016). Biofilms: an Emergent Form of Bacterial Life. *Nat. Rev. Microbiol.* 14, 563–575. doi:10.1038/nrmicro.2016.94

Gu, T., Jia, R., Unsal, T., and Xu, D. (2019). Toward a Better Understanding of Microbiologically Influenced Corrosion Caused by Sulfate Reducing Bacteria. *J. Mater. Sci. Technology* 35, 631–636. doi:10.1016/j.jmst.2018.10.026

Gu, T., and Xu, D. (2013). *Why Are Some Microbes Corrosive and Some Not? CORROSION 2013*. Paper No. 2336. Orlando, FL: NACE International.

Heidelberg, J. F., Seshadri, R., Haveman, S. A., Hemme, C. L., Paulsen, I. T., Kolonay, J. F., et al. (2004). The Genome Sequence of the Anaerobic, Sulfate-Reducing Bacterium *Desulfovibrio Vulgaris* Hildenborough. *Nat. Biotechnol.* 22, 554–559. doi:10.1038/nbt959

Jia, R., Wang, D., Jin, P., Unsal, T., Yang, D., Yang, J., et al. (2019). Effects of Ferrous Ion Concentration on Microbiologically Influenced Corrosion of Carbon Steel by Sulfate Reducing Bacterium *Desulfovibrio Vulgaris*. *Corrosion Sci.* 153, 127–137. doi:10.1016/j.corsci.2019.03.038

Jia, R., Yang, D., Al-Mahamedh, H. H., and Gu, T. (2017). Electrochemical Testing of Biocide Enhancement by a Mixture of D-Amino Acids for the Prevention of a Corrosive Biofilm Consortium on Carbon Steel. *Ind. Eng. Chem. Res.* 56, 7640–7649. doi:10.1021/acs.iecr.7b01534

Jogdeo, P., Chai, R., Shuyang, S., Saballus, M., Constancias, F., Wijesinghe, S. L., et al. (2017). Onset of Microbial Influenced Corrosion (MIC) in Stainless Steel Exposed to Mixed Species Biofilms from Equatorial Seawater. *J. Electrochem. Soc.* 164, C532–C538. doi:10.1149/2.0521709jes

Li, H., Xu, D., Li, Y., Feng, H., Liu, Z., Li, X., et al. (2015). Extracellular Electron Transfer Is a Bottleneck in the Microbiologically Influenced Corrosion of C1018 Carbon Steel by the Biofilm of Sulfate-Reducing Bacterium *Desulfovibrio Vulgaris*. *PLoS One* 10, e0136183. doi:10.1371/journal.pone.0136183

Li, X., Lan, S.-m., Zhu, Z.-p., Zhang, C., Zeng, G.-m., Liu, Y.-g., et al. (2018a). The Bioenergetics Mechanisms and Applications of Sulfate-Reducing Bacteria in Remediation of Pollutants in Drainage: a Review. *Ecotoxicology Environ. Saf.* 158, 162–170. doi:10.1016/j.ecoenv.2018.04.025

Li, Y., Xu, D., Chen, C., Li, X., Jia, R., Zhang, D., et al. (2018b). Anaerobic Microbiologically Influenced Corrosion Mechanisms Interpreted Using Bioenergetics and Bioelectrochemistry: a Review. *J. Mater. Sci. Technology* 34, 1713–1718. doi:10.1016/j.jmst.2018.02.023

DATA AVAILABILITY STATEMENT

The datasets generated for this study are available upon request to the corresponding author.

AUTHOR CONTRIBUTIONS

All authors listed have made a substantial, direct, and intellectual contribution to the work and have approved it for publication.

FUNDING

ACKNOWLEDGMENTS

Little, B. J., and Lee, J. S. (2007). *Microbiologically Influenced Corrosion*. Hoboken, New Jersey, United States: John Wiley & Sons. doi:10.1002/9783527610426.bard040603

Liu, H., Gu, T., Zhang, G., Liu, H., and Cheng, Y. F. (2018). Corrosion of X80 Pipeline Steel under Sulfate-Reducing Bacterium Biofilms in Simulated CO2-saturated Oilfield Produced Water with Carbon Source Starvation. *Corrosion Sci.* 136, 47–59. doi:10.1016/j.corsci.2018.02.038

Lv, M., and Du, M. (2018). A Review: Microbiologically Influenced Corrosion and the Effect of Cathodic Polarization on Typical Bacteria. *Rev. Environ. Sci. Biotechnol.* 17, 431–446. doi:10.1007/s11157-018-9473-2

Ning, J., Zheng, Y., Young, D., Brown, B., and Nešić, S. (2014). Thermodynamic Study of Hydrogen Sulfide Corrosion of Mild Steel. *Corrosion* 70 (4), 375–389. doi:10.5006/0951

Peck, H. D. (1993). "Bioenergetic Strategies of the Sulfate-Reducing Bacteria," in *The Sulfate-Reducing Bacteria: Contemporary Perspectives*. Editors J. M. Odom and R. Singleton (New York, NY: Springer), 41–76. doi:10.1007/978-1-4613-9263-7_3

Sheng, X., Ting, Y.-P., and Pehkonen, S. O. (2007). The Influence of Sulphate-Reducing Bacteria Biofilm on the Corrosion of Stainless Steel AISI 316. *Corrosion Sci.* 49, 2159–2176. doi:10.1016/j.corsci.2006.10.040

Służalec, A. (1992). "Stress-Strain Curve," in *Introduction to Nonlinear Thermomechanics: Theory and Finite-Element Solutions*. London: Springer London, 45–47. doi:10.1007/978-1-4471-1906-7_5

Wang, D., Liu, J., Jia, R., Dou, W., Kumseranee, S., Punpruk, S., et al. (2020). Distinguishing Two Different Microbiologically Influenced Corrosion (MIC) Mechanisms Using an Electron Mediator and Hydrogen Evolution Detection. *Corrosion Sci.* 177, 108993. doi:10.1016/j.corsci.2020.108993

Wu, T., Yan, M., Zeng, D., Xu, J., Sun, C., Yu, C., et al. (2015). Stress Corrosion Cracking of X80 Steel in the Presence of Sulfate-Reducing Bacteria. *J. Mater. Sci. Technology* 31, 413–422. doi:10.1016/j.jmst.2014.08.012

Xu, D., and Gu, T. (2011). *Bioenergetics Explains when and Why More Severe MIC Pitting by SRB Can Occur*. CORROSION 2011, Paper No. 11426. Houston, TX: NACE International.

Xu, D., and Gu, T. (2014). Carbon Source Starvation Triggered More Aggressive Corrosion against Carbon Steel by the *Desulfovibrio Vulgaris* Biofilm. *Int. Biodeterioration Biodegradation* 91, 74–81. doi:10.1016/j.ibiod.204.03.01410.1016/j.ibiod.2014.03.014

Xu, D., Li, Y., and Gu, T. (2016). Mechanistic Modeling of Biocorrosion Caused by Biofilms of Sulfate Reducing Bacteria and Acid Producing Bacteria. *Bioelectrochemistry* 110, 52–58. doi:10.1016/j.bioelechem.2016.03.003

Yin, K., Liu, H., and Cheng, Y. F. (2018). Microbiologically Influenced Corrosion of X52 Pipeline Steel in Thin Layers of Solution Containing Sulfate-Reducing Bacteria Trapped under Disbonded Coating. *Corrosion Sci.* 145, 271–282. doi:10.1016/j.corsci.2018.10.012